Chemical Physics Impact 5 (2022) 100110

Contents lists available at ScienceDirect

Chemical Physics Impact

journal homepage: www.sciencedirect.com/journal/chemical-physics-impact

The impact of functionals on $BiGaO_3$ structural, electronic, optical and thermoelectric properties

K. Bouferrache [a,b], L. Krache [c], M.A. Ghebouli [d,e], B. Ghebouli [f], Sameh I. Ahmed [g], M. Fatmi [c,*], T. Chihi [c], B. Gueridi [h]

[a] Department of Physics, Faculty of Science, University of Mohamed Boudiaf, M'sila 28000, Algeria
[b] Laboratory of Physics and Chemistry of Materials, University of Mohamed Boudiaf, M'sila 28000, Algeria
[c] PQSD Laboratory, Department of Physics, Faculty of Science, University Ferhat Abbas of Setif 1, Setif 19000, Algeria
[d] Department of Chemistry, Faculty of Technology, University of Mohamed Boudiaf, M'sila 28000, Algeria
[e] Research Unit on Emerging Materials (RUEM), University of Setif 1, 19000, Algeria
[f] Laboratory of Studies Surfaces and Interfaces of Solids Materials, Department of Physics, Faculty of Science, University Ferhat Abbas of Setif 1, Setif 19000, Algeria
[g] Department of Physics, College of Science, Taif University, P.O. Box 11099, Taif 21944, Saudi Arabia
[h] Department of Biology, Faculty of Natural and Life Sciences, University Ferhat Abbas of Setif 1, Setif 19000, Algeria

ARTICLE INFO

Keywords:
Band gaps
mBJ-LDA
mBJ-GGA
$BiGaO_3$

ABSTRACT

The functionals mBJ-LDA and mBJ-GGA result in high band gaps. $BiGaO_3$ contains covalent bonds due to the mixing of O **2p** states with the Bi and Ga **s,p** states. The Bi breadth PDOS was obviously less in the valence band region compared to Ga and O, with fewer peaks than there were for Ga and consequently Ga-O hybridization is more powerful than Bi-O hybridization. All optical spectra obtained by using mBJ-GGA and EV-GGA approaches have the same profile. At the same energy as the indirect M-X band gap values of 2.24 and 2.56 eV for EV-GGA and mBJ-GGA, the imaginary component reaches non-zero magnitude. The increase in temperature from 300 to 800 K reduces the Seebeck coefficient in $BiGaO_3$ from (3000 to 1500) μV/K. As p-type and n-type ZT have similar values, $BiGaO_3$ has the same thermoelectric efficiency whether it is p-type or n-type.

1. Introduction

The search for sustainable and environmentally energy resources involves the use of thermoelectric materials that convert waste heat into electricity. A ferroelectric material with significant piezoelectric responses [3] and high polarizations is bismuth gallium oxide [1,2]. The substantial ion off-centering and consequently large ferroelectric polarization in Bi-based perovskites are caused by the stereochemically active $6s^2$ lone pair on the Bi^{3+} ions. This material can exist in several phases, where we quote the cubic, rhombohedral, orthorhombic, monoclinic and tetragonal. $BiGaO_3$ is characterized by smaller reticular distances, higher Coulomb forces and quite significant elastic constants [4]. By studying the formation of enthalpy, L. Krache et al. quoted a transition from the Pcca phase to R3c at a pressure of 5 GPa [4]. Phase transitions are brought on by crystal anisotropy and the relative displacement of atoms in the R3c phase compared to the Pcca phase. Experiment results on $BiGaO_3$ material confirm the pyroxene structure with space group Pcca. By using the sol–gel method, the elaborated nanocrystalline $BiGaO_3$ films have orthorhombic structure [5]. $BiFeO_3$ transitions from a rhombohedral to an orthorhombic phase as a result of hydrostatic pressure [6]. An indirect band gap value of 2.17 eV was measured on $BiGaO_3$ by ellipsometric method, which made it suitable for photovoltaic devices. According to ellipsometric tests, $BiGaO_3$ has an indirect band gap with a value of 2.17 eV, which made it suitable for photovoltaic devices [5]. Sajad Ahmad Dar et al. reported that $MBiO_3$(M =Rb, Cs, Tl) were studied as thermoelectric materials [7]. $BiGaO_3$ can be synthesized under high temperatures and pressures [8]. The phase transitions from pyroxene Pcca to monoclinic cm, monoclinic cm to rhombohedral R3c, and R3c to Pnma take place at 3.5 GPa, 5.2 GPa, and 7.4 GPa, respectively [9]. Piezoelectricity, ferroelectricity, anti-ferromagnetism, and super-conductivity are only a few of the useful properties of $BiGaO_3$. The difference between our work and others lies in the fact that the thermoelectric properties were treated for the first time. In addition, this work was characterized by the WIEN2k code, whereas, the other works were carried out by CASTEP. Anisotropic behavior of $BiGaO_3$'s optical property is discovered [10]. $BiGaO_3$ exhibits optical

* Corresponding author.
E-mail address: fatmimessaoud@yahoo.fr (M. Fatmi).

https://doi.org/10.1016/j.chphi.2022.100110
Received 16 August 2022; Received in revised form 24 September 2022; Accepted 30 September 2022
Available online 3 October 2022

Table 1
The values of $R_{MT}xK_{max}$, R_{MT} of each constituent and k-point of $BiGaO_3$ using GGA and LDA.

Compound	Approach	$R_{MT}xK_{max}$	R_{MT} (Bi)	R_{MT} (Ga)	R_{MT} (O)	k-point
$BiGaO_3$	**GGA**	9	2.50	1.73	1.56	3000

Table 2
Equilibrium lattice constant, bulk modulus and its pressure derivative and cohesive energy of $BiGaO_3$ calculated within GGA and LDA approximations.

Compound	Parameters	GGA	LDA
$BiGaO_3$	*a* (Å)	3.90	3.8152
	B (GPa)	171.7216	209.8554
	B'	4.4913	4.8329
	E_{min} (Ry)	-47502.938267	-47471.70692

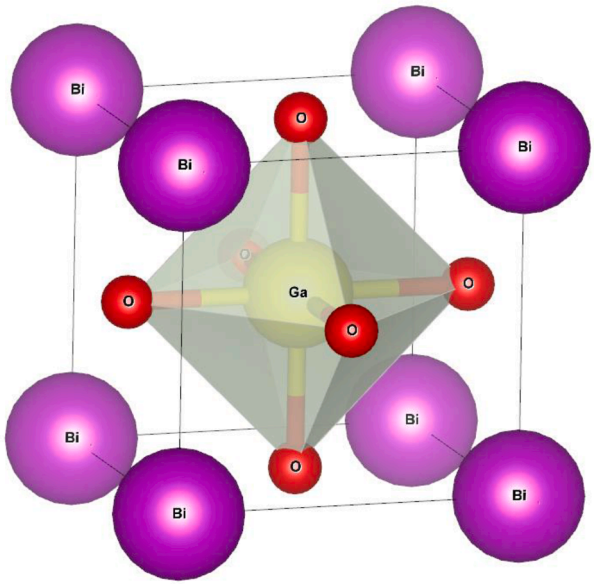

Fig. 1. Schematic representation of $BiGaO_3$structure.

properties that span the full visible spectrum and a portion of the UV spectrum. It is a viable contender for photovoltaic solar cells and optoelectronic devices due to its exceptional carrier mobility and high optical performance [11]. The studied compound has a small indirect energy gap, which is one of the features interested in studying photovoltaic. The maximum of optical conductivity is 7500 $(\Omega.cm)^{-1}$ in the field 5 to 15 electron volts, and also the absorption coefficient is 22.5 × 10^5 cm^{-1} for higher energy. These characteristics make it possible to consider this compound as candidate for application as an absorber in photovoltaic cells. Our calculation shows that $BiGaO_3$ is intrinsic semiconductor, its band gap is in the range 1.396–2.855 eV for various functionals, this makes them a good contender for optoelectronic and photovoltaic applications. $BiGaO_3$ possesses higher Seebeck coefficient compared to conventional thermoelectric materials confirming its potentiality as a thermoelectric device. Thermoelectric materials are considered to be excellent as candidates as energy sources [12]. This work describes the effects of functionals on the structural, electronic band structures, optical, and thermoelectric properties of $BiGaO_3$ under high pressure. We organize the paper such as the calculation detail is provided in the Section 2. We present the computed results and discus them in the Section 3. We close the paper with brief conclusion in the last section.

2. Calculation model

The calculations were performed by employing the augmented plane-wave plus local orbitals basis functions as embodied in the WIEN2k code and GGA+U and LDA+U approximations [13]. The code used for calculations of thermoelectric properties is Boltztrap. It was written by G.K.H. Madsen and D. J. Singh, as detailed in the Ref. [14].

The GGA, mBJ-GGA, EV-GGA, LDA and mBJ-LDA approximations are used as potential exchange-correlation in the calculation of the structural, electronic, optical and thermoelectric properties [15,16]. The exchange potentials that are used in the stationary state as GGA and LDA give electronic and optical properties close to the experimental one. GGA is the best used in semiconductors, while LDA is used in the study of metals. GGA+U, LDA+U, mBJ and HSE06 are used in the excited state. The most accurate functional turned out to be the popular modified (mBJ-LDA) correlation and (mBJ-GGA) potential [17] followed very closely by the GGA high-local exchange (HLE16) and the screened hybrid HSE06 [18]. The framwork of density functional theory (DFT) with newly developed EV-GGA and EV-LDA. These potentials go beyond the LDA and GGA. They show improved energy band gap and optical constants [19]. The electronic properties are determined using the modified Becke-Johnson approach [20]. The electron-electron correlation effect is treated by the DFT+U approximation [21]. The charge density and potential are expressed using the spherical harmonic expansion with angular moments up to I_{max}= 10. R_{MT} K_{max} = 9 (R_{MT} is the smallest of all atomic sphere radii and K_{MAX} is the cutoff of the interstitial plane wave) and a sampling of 3000 k-points in the irreducible region of the Brillouin zone are used to control the plane-wave expansion (BZ). The separation between the core and valence states occurs at the energy cut-off value of 8.0 Ry. 0.001 e was used for charge convergence.

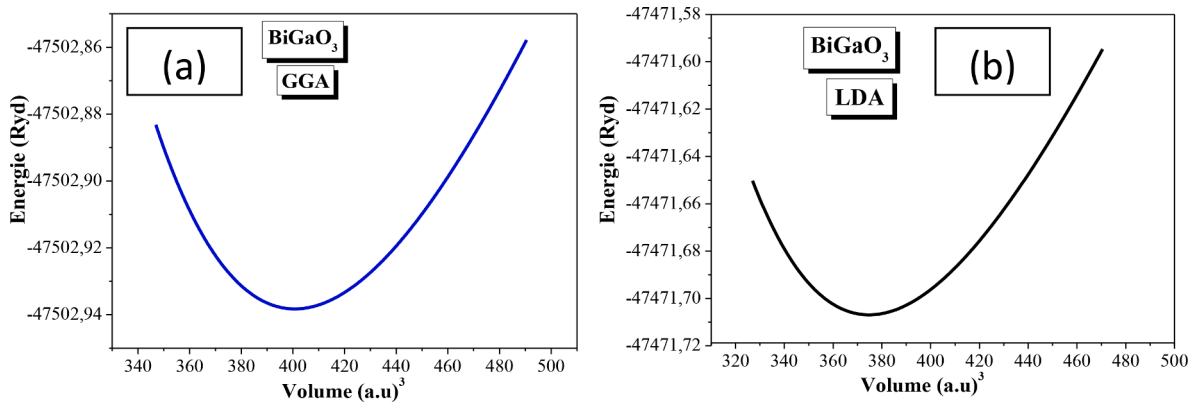

Fig. 2. Variation of total energiesas a function of volume for $BiGaO_3$ using(a) GGA and (b)LDA.

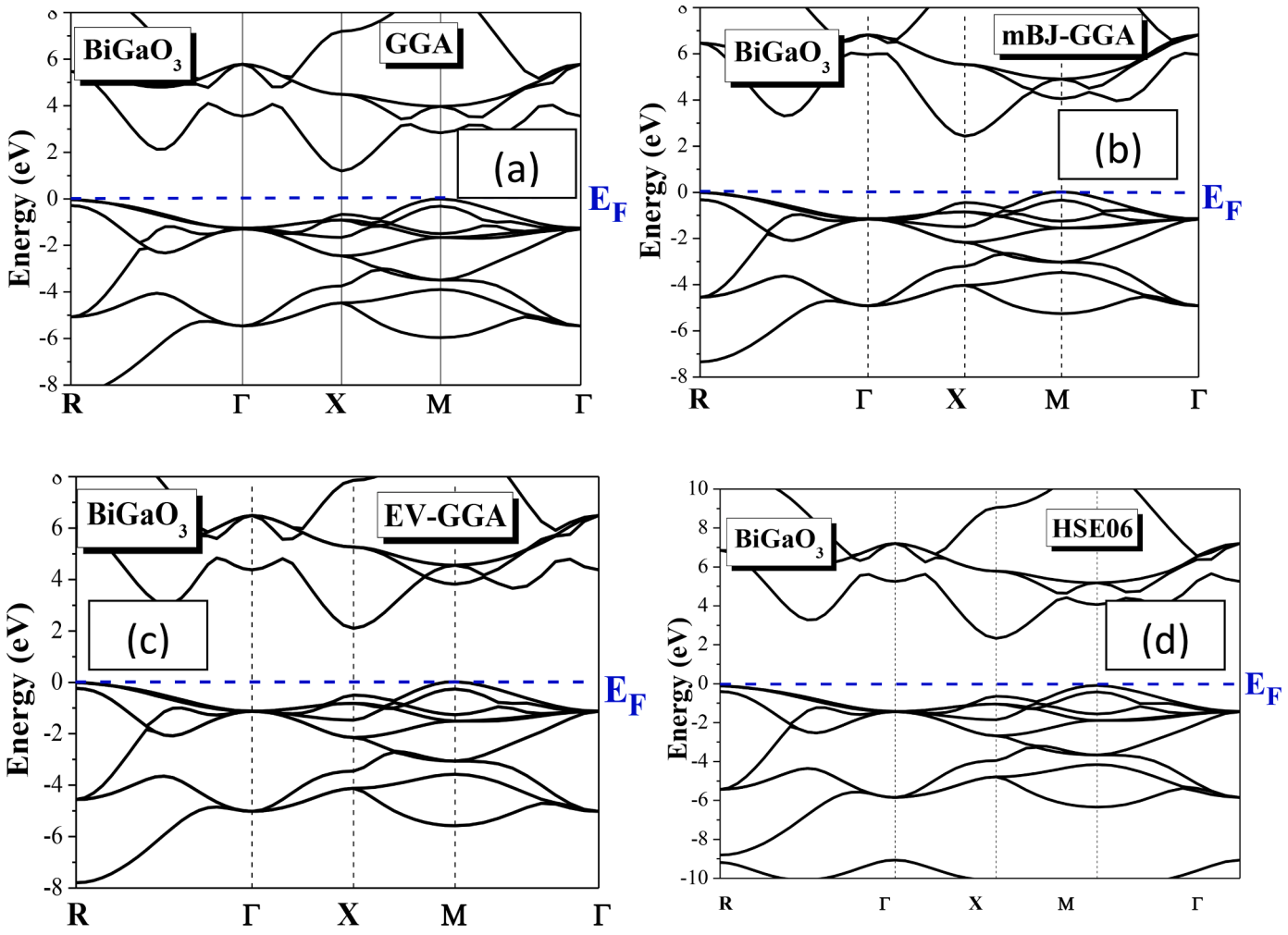

Fig. 3. Electronic band structures of $BiGaO_3$using (a) GGA, (b) mBJ-GGA(c)EV-GGA and(d) HSE06functionals.

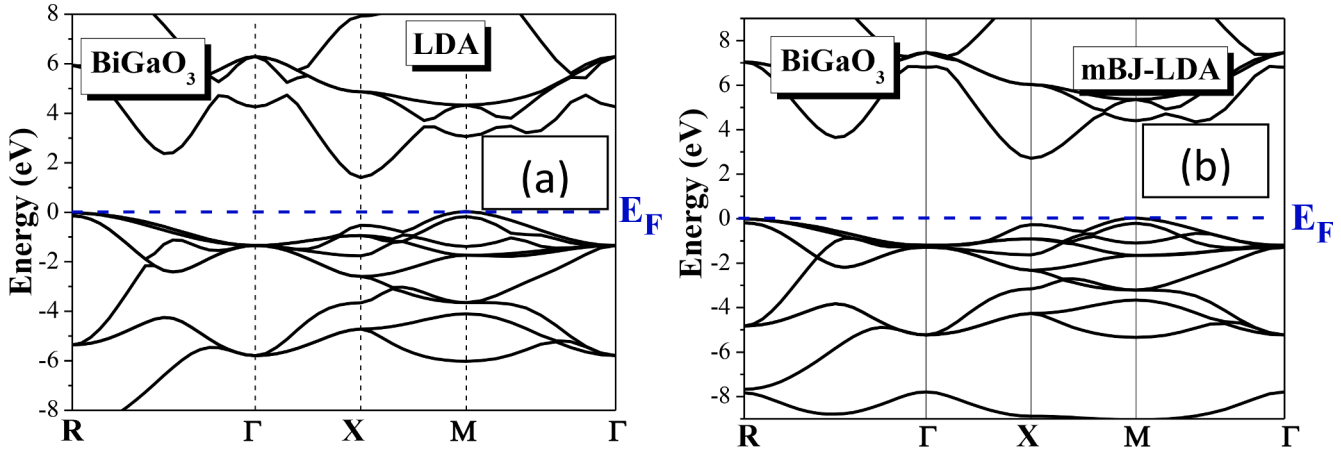

Fig. 4. Electronic band structures of $BiGaO_3$ using (a) LDA, (b) mBJ-LDA.

3. Results and discussions

3.1. Structural properties

The structural behavior of $BiGaO_3$ in Pm-3m (221) phase is studied using GGA and LDA approximations. The atomic positions of Bi, Ga and O are (0,0,0), (0.5,0.5,0.5) and (0,0.5,0.5). Table 1 shows the values of $R_{MT}xK_{max}$, R_{MT}(Bi), R_{MT}(Ga) and R_{MT}(O) and **k-point** of $BiGaO_3$ using GGA and LDA. The lattice constant, bulk modulus, and its pressure derivative are determined using the GGA and LDA techniques and are shown in Table 2. Closer to the theoretical GGA (LDA) value of 3.8988 Å (3.8147 Å) [4] is the lattice constant. The crystal structure of the Pm-3m phase of $BiGaO_3$ is visualized in Fig. 1. We represent in Fig. 2 the volume effect on the total energies of $BiGaO_3$ at ambient pressure using GGA and

Table 3
The band gap for of $BiGaO_3$ using GGA, mBJ-GGA, EV-GGA, LDA, mBJ-LDA and HSE06.

Functional	Band gap
GGA	1.396 eV
mBJ-GGA	2.567 eV
EV-GGA	2.241 eV
LDA	1.594 eV
mBJ-LDA	2.855 eV
HSE06	2.357 eV

LDA. The stability is more pronounced using LDA approach. The LDA gives lower lattice constant and high bulk modulus. The formation energy, cohesive energy and tolerance factors ensure the stability of compounds in cubic phase [22].

3.2. Band structure and density of states

The results of the electronic band structure of $BiGaO_3$ using GGA, mBJ-GGA, EV-GGA and LDA and mBJ-LDA functionals are shown in Figs. 3 and 4. All functional bands have a similar shape, and the band gap is an indirect M→X. The indirect band gap of $BiGaO_3$ using GGA, mBJ-GGA, EV-GGA, LDA and mBJ-LDA are illustrated in Table 3. The band gap values in $BiGaO_3$ is 1.015 eV, 1.144 eV and 1.893 eV for GGA, spin polarized and HSE functional, respectively [23]. According to the bonding characteristics, the energy bands can be classified into a number of areas. mBJ-GGA and mBJ-LDA functionals give a high gap, there is no experimental value. The full and partial state densities of $BiGaO_3$ as determined using GGA, EV-GGA, mBJ-GGA, LDA and mBJ-LDA are shown in Figs. 5 and 6 respectively. The top of the valence band (VB) and the bottom of the conduction band (CB) are composed of **O-2p** states and **Bi-6p** states, respectively. The **O-2p** density of states at the upper valence band is greater for mBJ-GGA and EV-GGA (mBJ-LDA) compared with GGA (LDA). We see that the O-**2p** states have some admixture with the Bi-**pd** and Ga-**pd** states, leading to certain covalent characteristics in $BiGaO_3$. Additionally, the breadth of the PDOS of Bi was obviously less in the valence band region than that of Ga and O. Additionally, there were fewer peaks than there were for Ga. This shows that Ga-O hybridization is more powerful than Bi-O hybridization. Covalent and ionic bonding behaviors are combined in $BiGaO_3$'s bonding activity. The covalent bonding strength of the Ga-O bond is greater than that of the Bi-O bond.

We report the partiel density of states for all atoms in $BiGaO_3$ using EV-GGA functional in Fig. 7. The O contribution is due to **s** and **p** sites. **p, d** and **f** sites contribute to Ga and Bi. The first conduction band is vacant between Fermi's level and 3 eV.

3.3. Optical properties

Using mBJ-GGA and eV-GGA, Fig. 8 (a)–(h) reports the absorption coefficient, optical conductivity, energy loss spectra, real and imaginary parts of the dielectric function, reflectivity spectra, refractive index, and the extinction coefficient as a function of photon energy for in-plane [100] crystallographic direction. In the ultraviolet spectrum between

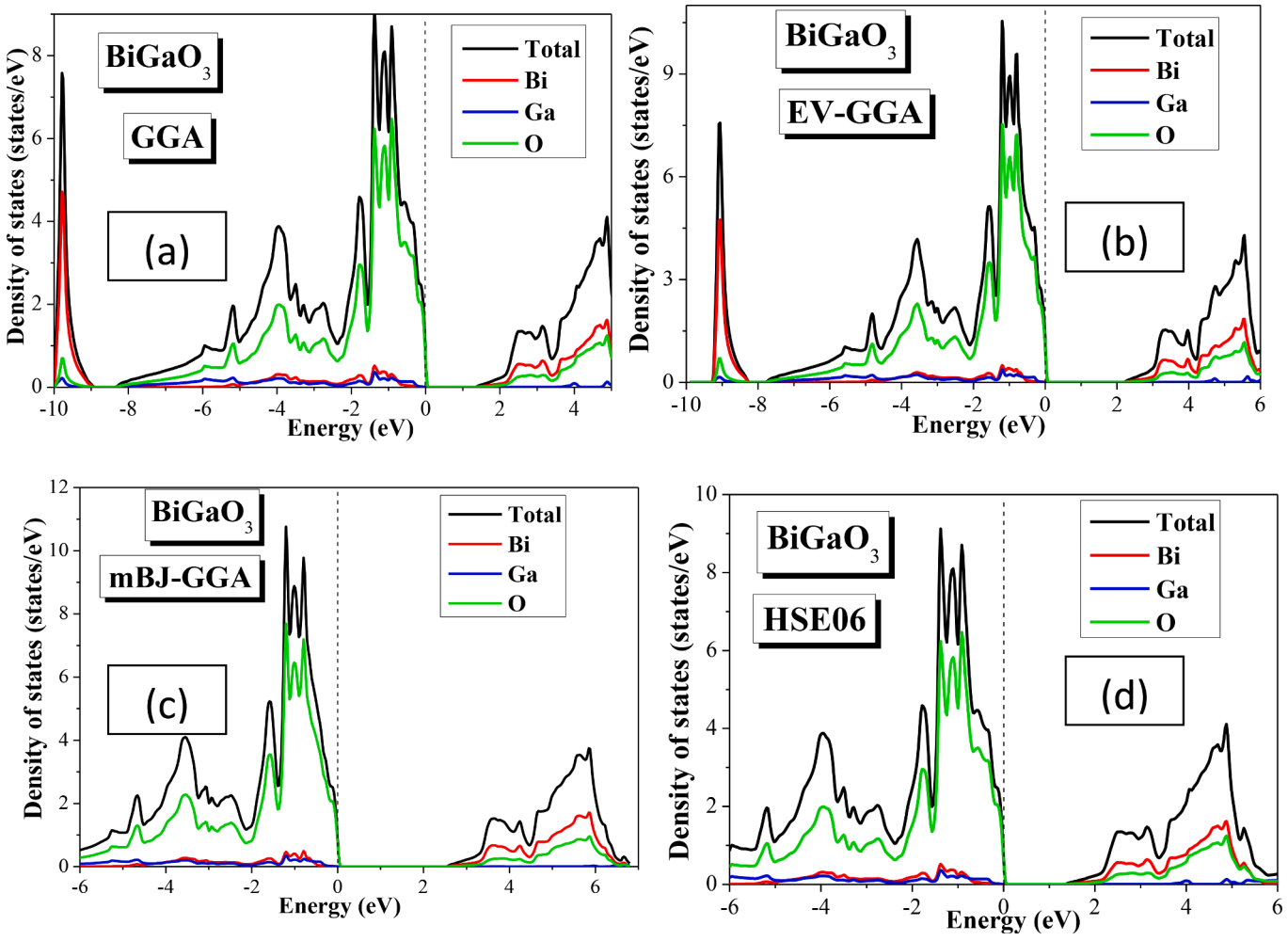

Fig. 5. The total and partial density of states for $BiGaO_3$ using (a)GGA, (b) mBJ-GGA, (c)EV-GGA and (d) HSE06 functionals.

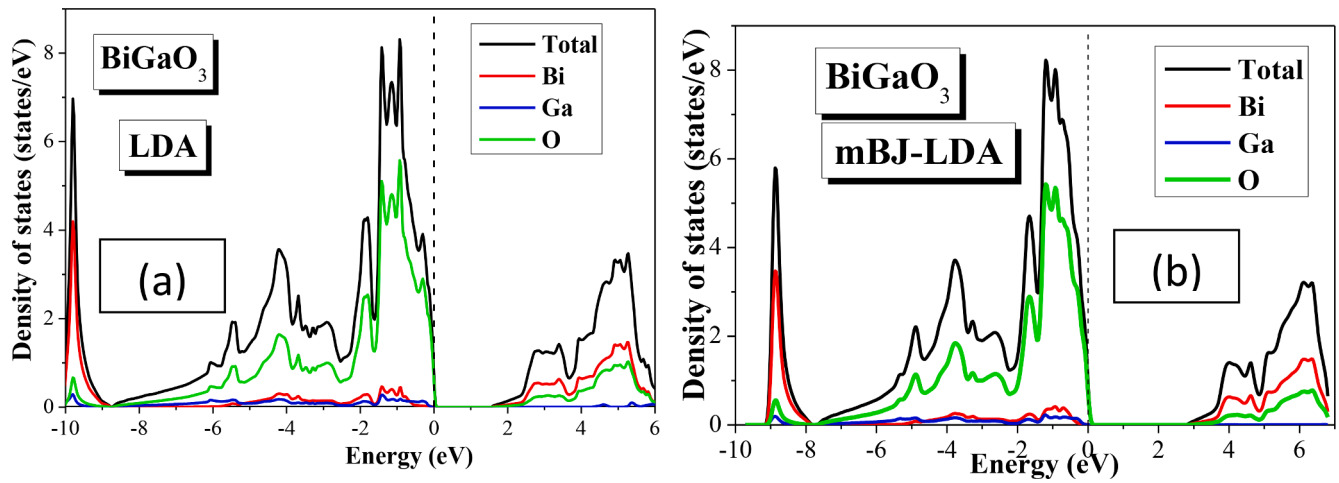

Fig. 6. The total and partial density of states for $BiGaO_3$ using (a)LDA and (b) mBJ-LDA functionals.

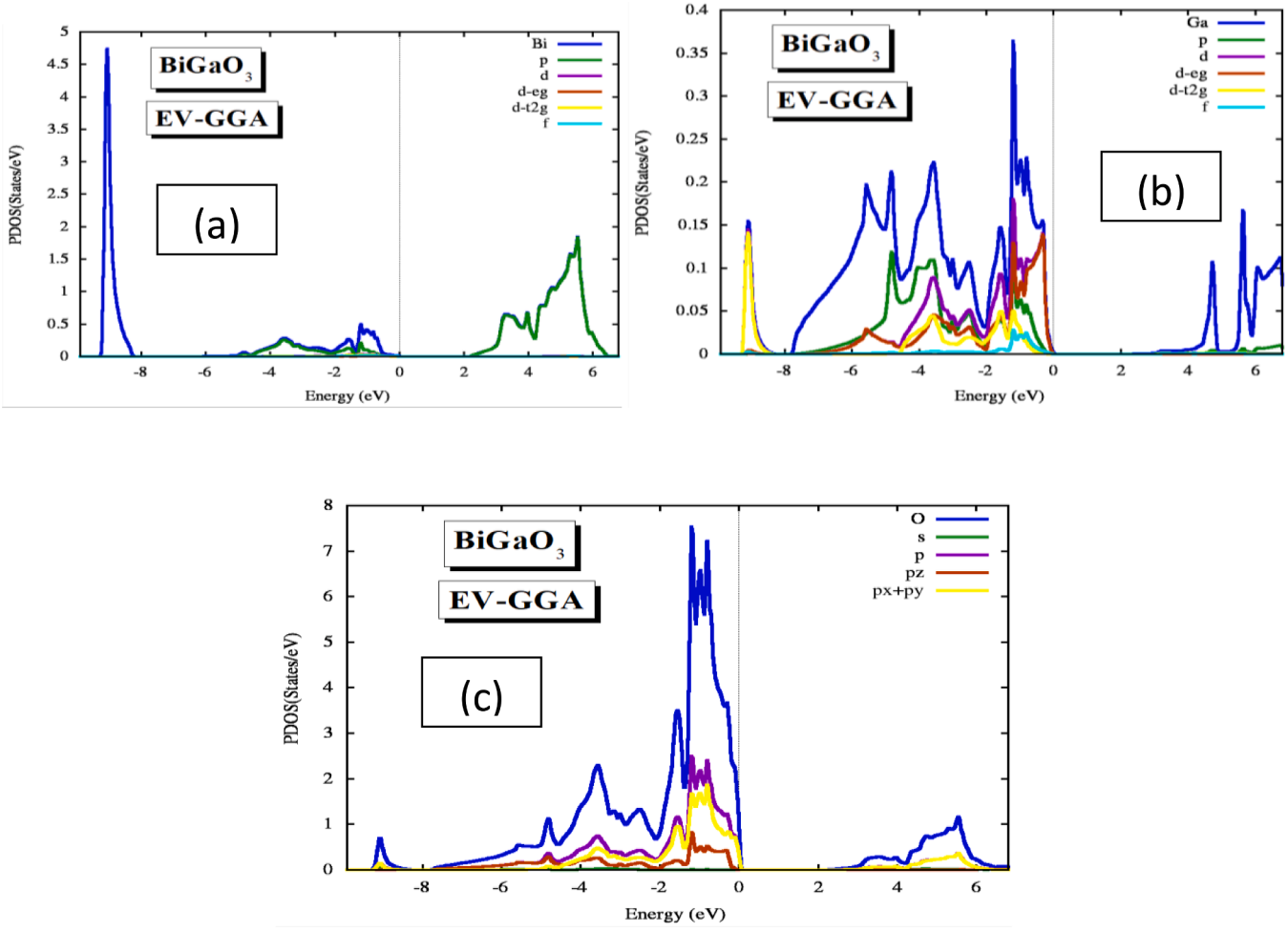

Fig. 7. The partial density of states for (a) Bi, (b) Ga and (c) O atoms usining EV-GGA functional.

5 and 20 eV, $BiGaO_3$ absorbs light. This development confirms its suitability for photovoltaic and photonic systems. It is emphasized that $BiGaO_3$ has a 22.5 $\times$ 10^5 cm^{-1} absorption coefficient, which is a desirable quality in an absorber material. The maximum of optical conductivity is 7500 $(\Omega.cm)^{-1}$ obtained in the range 5 to 15 eV. The maximum of optical conductivity [7500 $(\Omega.cm)^{-1}$], the absorption coefficient (22.5 $\times$ 10^5 cm^{-1}) make $BiGaO_3$ as candidate for application as an absorber in photovoltaic cells. The photonic band structure of the crystal is connected to the characteristics of the energy-loss spectrum. The electron's contact with the crystal results in energy loss. The area of UV light is where the electron energy loss is concentrated. All spectra obtained by using mBJ-GGA and EV-GGA approaches have the same profile. The static real part is 6, 6.7 and 10 for mBJ-GGA, EV-GGA and HSE06. It becomes zero at 4, 6 and 6.5 eV for HSE, EV-GGA and mBJ-

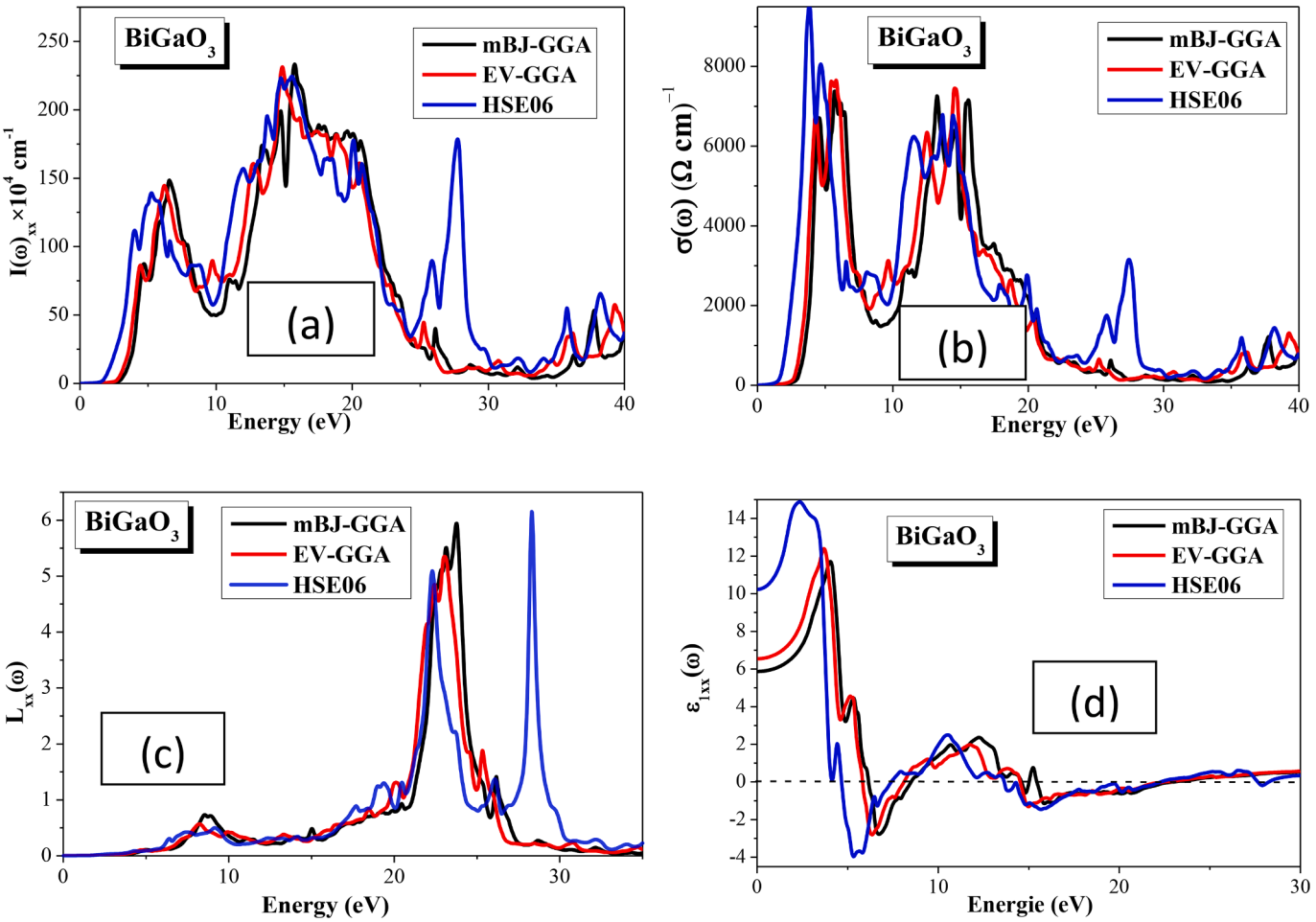

Fig. 8. The absorption coefficient (a), the optical conductivity (b), the energy loss spectra(c),the real part of the dielectric function(d),the imaginary part of the dielectric function(e),the reflectivity spectra(f),the refractive index(g), the extinction coefficient(h) as a function of energy for $BiGaO_3$ using mBJ-GGA; EV-GGA and HSE06.

GGA. The actual dielectric function aids in forecasting the material's nonlinear optical behavior. The static dielectric constant $\varepsilon_1(0)$ value of mBJ-GGA is smaller than that of HSE06, with parallel polarization implying smaller conductivity and carrier mobility of mBJ-GGA compare to HSE06 [24]. The absorptive capability of such a material is represented by the fictitious portion of the dielectric function. We can observe that the imaginary component attains non-zero magnitude at energy identical of that corresponding to the indirect M-X band gap values of 2.24 eV and 2.56 eV for eV-GGA and mBJ-GGA. The optical band gap, which is the threshold for the optical transition between VBM and CBM, is represented by the first peak of $\varepsilon_2(\omega)$. The origin of the absorption peak can be attributed to the electronic transitions from DOS spectra. Strong light-matter interactions caused by the presence of several van Hove singularities (VHSs) in the DOS increase photon absorption [11]. Due to its low reflectance and strong UV transparency, $BiGaO_3$ is suggested for usage in solar cells as it greatly lowers optical loss [25]. $BiGaO_3$ shows optical features covering the entire visible region and a part of the UV region as well. The material is not capable of photon emission due to the intense peak's location at 3.5 eV, which signals an inter band transition. The first edge value of this quantity was 0.2 and the magnitude attain the maximum at 25 nm, which was outside the visible region, It reaches a number of maximum and minimum peaks in the area of UV light. The material's refractive index gauges how transparent it is to incoming spectrum radiation. For EV-GGA and mBJ-GGA, the static refractive index is 2.4 and 2.6, respectively. It is discovered that $BiGaO_3$ has an anisotropic optical characteristic.

3.4. Thermoelectric properties

The figure of merit ZT, which is defined as [25] $ZT = \frac{GS^2T}{k_e+k_{ph}}$ where G is the electrical conductance, S is the Seebeck coefficient, T is the temperature, k_e is the electronic part of thermal conductance and k_{ph} is the phonon contribution of thermal conductance. Strong ZT termoelectric materials have low thermal conductivity and high Seebeck and electrical conductance. Strong ZT termoelectric materials have low thermal conductivity and high Seebeck and electrical conductance. The transport properties of $BiGaO_3$ are investigated as a function of the chemical potential for three different temperatures (300 K, 600 K, and 800 K). The thermoelectric material has lattice stability, a mechanical thermal as well a high figure of merit (ZT). Thermal transport coefficients such as Seebeck coefficient, electrical condctivity, electronic thermal conductivity, figure of merite, power factor as a function of chemical potential at three fixed temperatures $T = 300$ K, 600 K and 800 K for $BiGaO_3$ using mBJ-GGA and EV-GGA are displayed in Figs. 9 (a)–(e) and 10 (a)–(e). The amplitude of an induced thermoelectric voltage in response to a temperature difference across a material is measured by the Seebeck coefficient, also known as thermoelectric sensitivity of a material. The flow of current between hot and cold electrodes is started by a material's temperature gradient, and as a result, an electric field and corresponding voltage, known as the Seebeck voltage, are created across the two ends. The greatest value of Seebeck, which is higher than that of traditional thermoelectric material, is 3000 μV/K at 300 K, corresponding to μ =

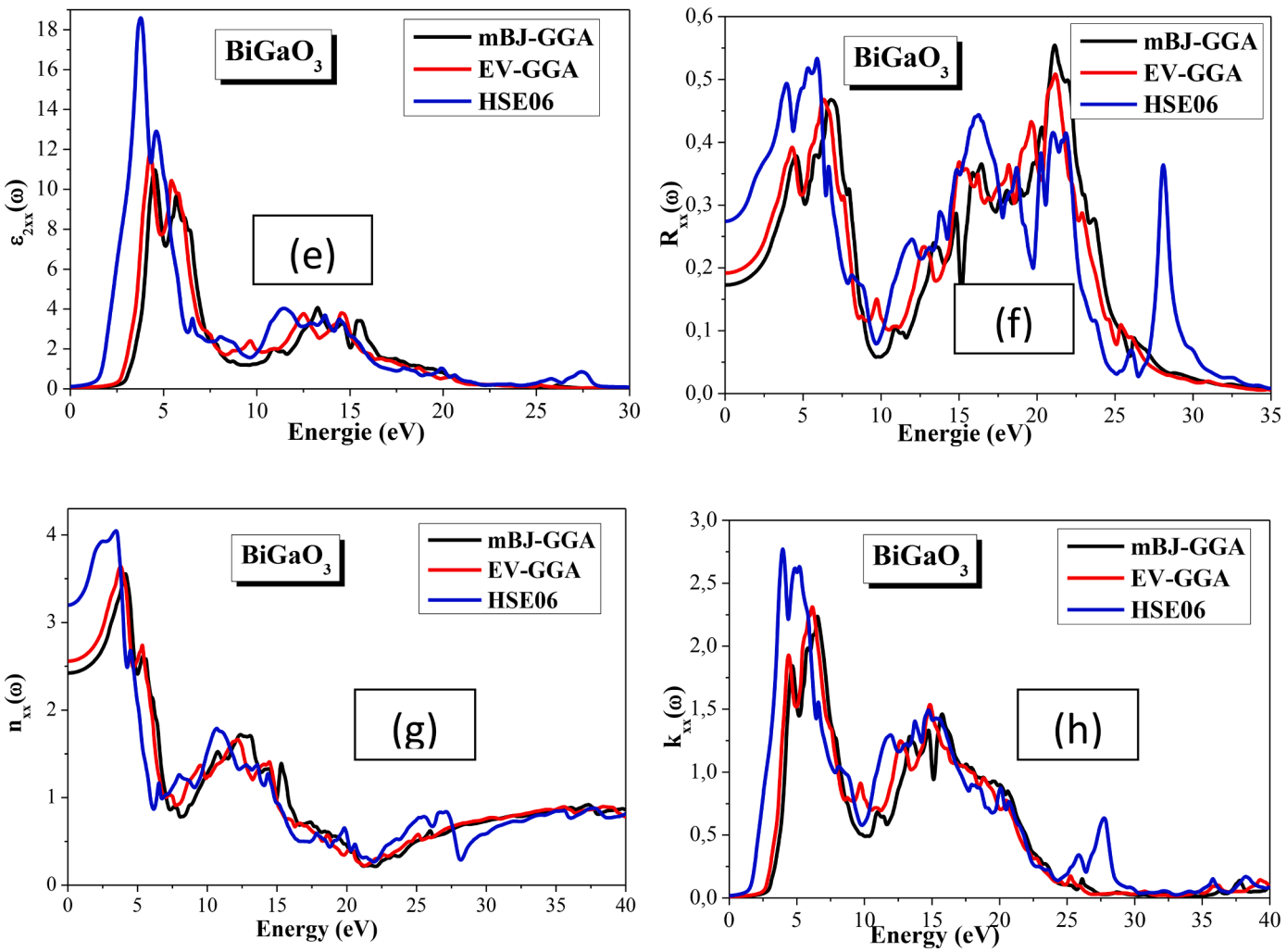

Fig. 8. (*continued*).

$\pm 0.7Ry$. Regardless of temperature, the Seebeck coefficient exhibits two peaks near the Fermi level that are virtually identical in value, demonstrating the isotropic nature of S. A system with a large band gap has a high S value because S and Eg are connected by: $S \approx -\frac{k_B}{e}\left(\frac{E_g}{2k_BT}+2\right)$. The substantial value of S in this system is a result of $BiGaO_3$'s broad band gap. The increase in temperature from 300 K to 800 K reduces the Seebeck coefficient in $BiGaO_3$ from (3000 to 1500) μV/K. For electrons and holes two-parabolic bands, where the Seebeck coefficient is slightly asymmetric as a result of the mass difference between electrons and holes. The total electrical conductivity of the p-type is less than the n-type. The overall electrical conductivity curves are less temperature sensitive. The use of a material in thermoelectric applications requires also a large magnitude of electrical conductivity. The highest electrical conductivity is 7×10^7 $(\Omega ms)^{-1}$ obtained at $\mu = -1.5Ry$. The total electronic conductivity of the p-type is less than the n-type. The total electronic conductivity curves are sensitive to the temperature. The total electronic conductivity increases with increasing temperature. In $BiGaO_3$, there is little electonic thermal conductivity. The highest $k_e$value is 10.4×10^2 (mKs) obtained at $\mu = -1.5Ry$for $T = 800$ K. According to the Wiedemann Franz law, the thermal conductance exhibits a similar pattern to the electrical conductance. Seebeck coefficient (electrical and thermal conductance) decreases (increases) with increase in temperature [11]. The competition between thermal transmission and electronic transfer is evaluated by the thermoelectric figure of merit, ZT (total thermal conductivity). Using the relationship $ZT_e = \frac{GS^2T}{k_e}$, we determined the thermoelectric figure of merit. We notice the presence of two plateaus around the Fermi level. $BiGaO_3$ has a small figure of merit. The increase in temperature from 300 to 800 K do not reduces the figure of merite in $BiGaO_3$. Using a constant relaxation time ($\tau = 10^{-13}$ s) and a constant phonon lattice thermal conductivity, the maximum ZT is computed. As p-type and n-type ZT have similar values, this material has the same thermoelectric efficiency whether it is p-type or n-type. The ratio of the real power absorbed by the load to the visible power flowing in the circuit is known as the power factor of a system. The n-type has a bigger power factor values than the p-type. The power factor increases with increasing temperature.

4. Conclusion

We studied the impact of functionals on the structural, electronic band structures, optical, and thermoelectric properties of $BiGaO_3$. The stability is more pronounced using LDA approach, which gives lower lattice constant and high bulk modulus. The bands of $BiGaO_3$ using GGA, mBJ-GGA, EV-GGA, LDA and mBJ-LDA have a similar form and the band gap is indirect M→X. **s** and **p** sites are responsible for the O contribution, while Ga and Bi are influenced by **p**, **d**, and f sites. $BiGaO_3$ absorbs ultraviolet light, which validates its candidature for optical and photovoltaic devices. The static refractive index is 2.4 and 2.6 for EV-GGA and mBJ-GGA. The Seebeck coefficient is slightly asymmetric as a result of the mass difference between electrons and holes. The total electronic conductivity of the p-type is less than the n-type and their curves are

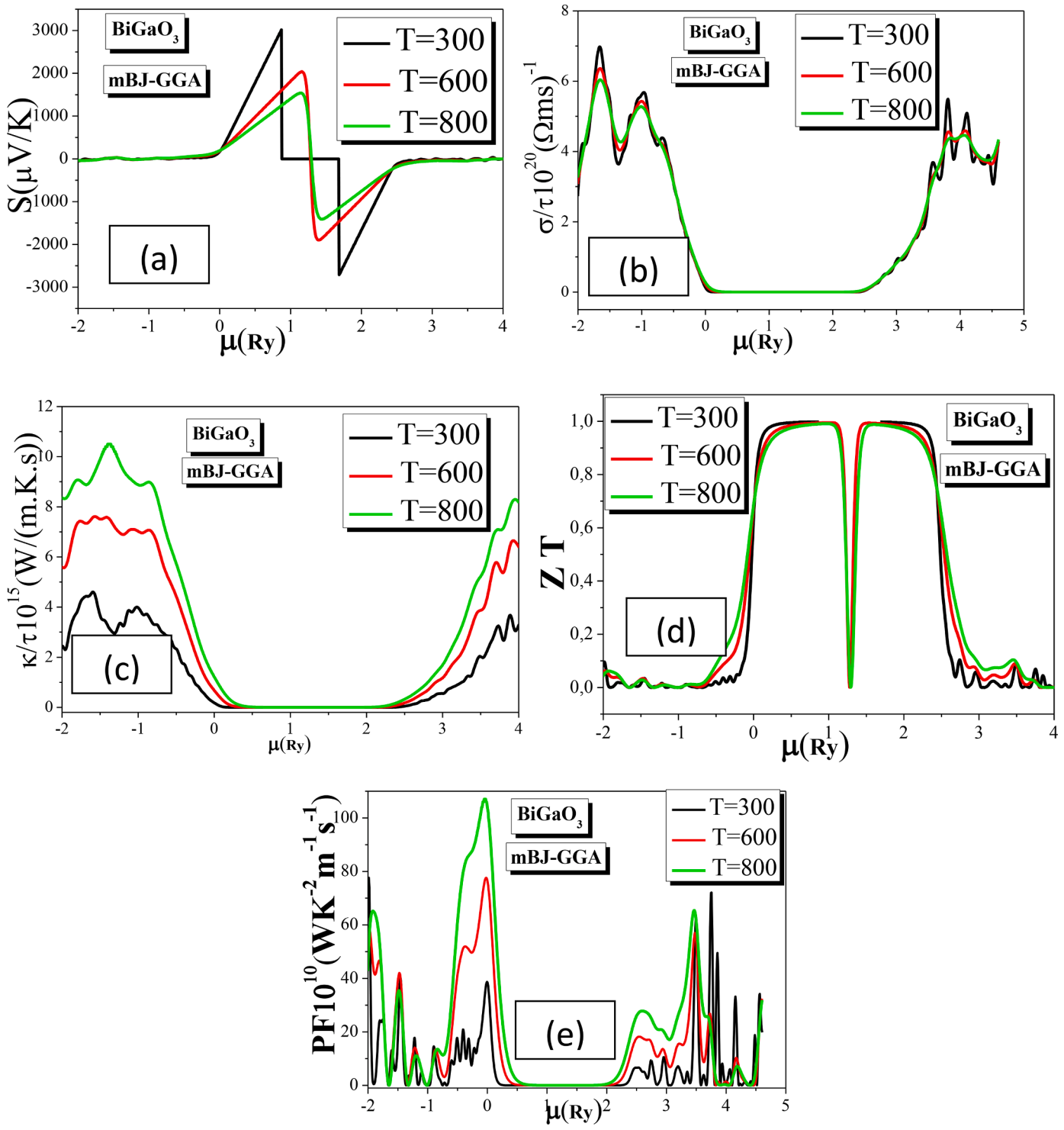

Fig. 9. The Seebeck coefficient (a), electrical condctivity (b), electronic thermal conductivity (c), figure of merite (d), Power factor (e) as a function of chemical potential at three fixed temperatures $T = 300$ K, 600 K and 800 K for $BiGaO_3$ using mBJ-GGA.

sensitive to the temperature. The power factor increases with increasing temperature.

Novelty statement

1- The bands of $BiGaO_3$ using GGA, mBJ-GGA, EV-GGA, LDA and mBJ-LDA have a similar form and the band gap is indirect M→X.
2- S and P sites are responsible for the O contribution, while Ga and Bi are influenced by P, d, and f sites.
3- $BiGaO_3$absorbs ultraviolet light, which validates its candidature for optical and photovoltaic devices.
4- The static refractive index is 2.4 and 2.6 for EV-GGA and mBJ-GGA.
5- The Seebeck coefficient is slightly asymmetric as a result of the mass difference between electrons and holes.

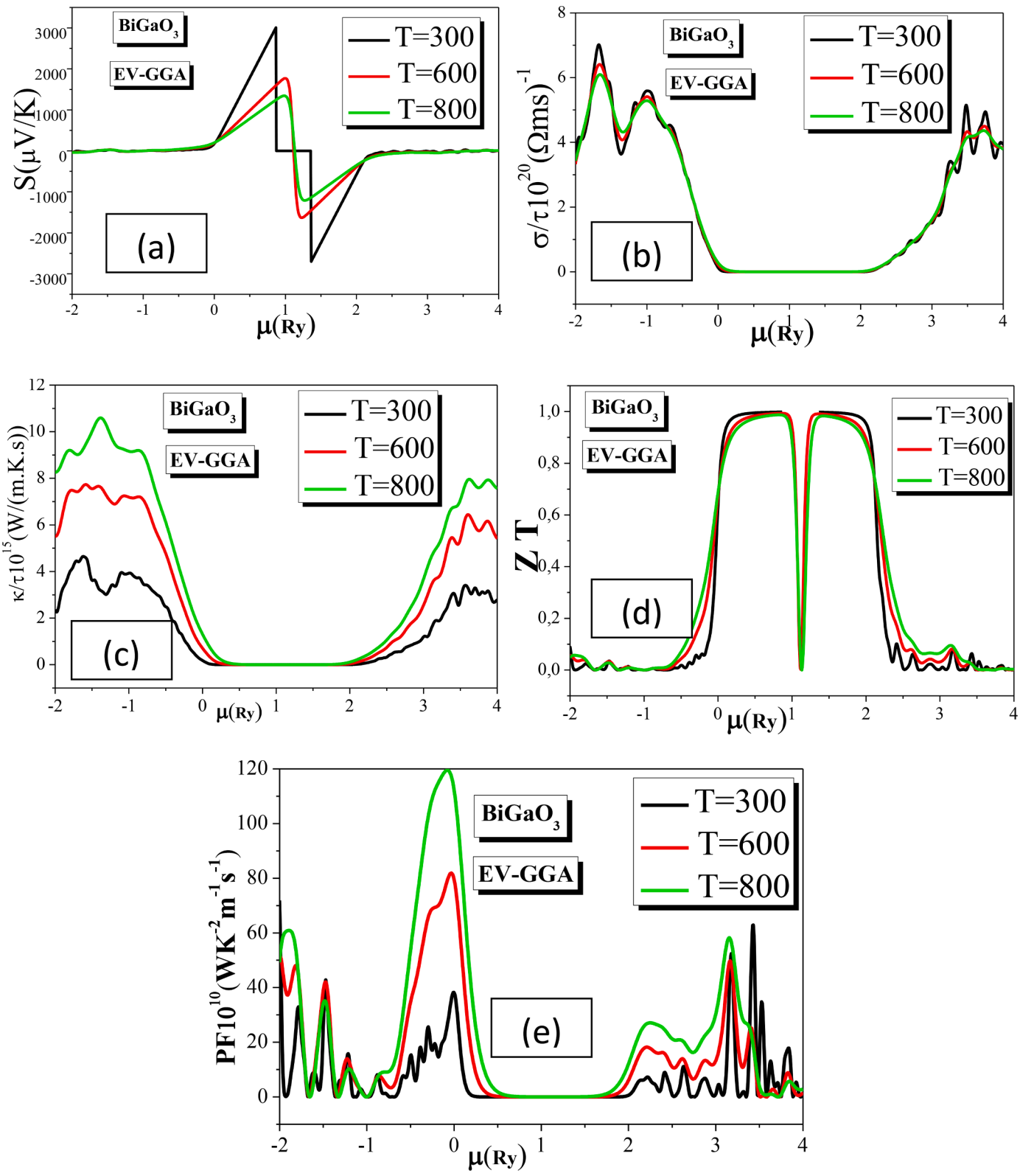

Fig. 10. The Seebeck coefficient (a), electrical condctivity (b), electronic thermal conductivity (c), figure of merite (d), Power factor (e) as a function of chemical potential at three fixed temperatures T = 300 K, 600 K and 800 K for $BiGaO_3$ using EV-GGA.

6- The total electronic conductivity of the p-type is less than the n-type and their curves are sensitive to the temperature.

CRediT authorship contribution statement

K. Bouferrache: Investigation. **L. Krache:** Writing – original draft. **M.A. Ghebouli:** Data curation. **B. Ghebouli:** Formal analysis, Writing – review & editing. **Sameh I. Ahmed:** Project administration, Resources, Software, Visualization. **M. Fatmi:** Conceptualization, Funding acquisition, Methodology. **T. Chihi:** Supervision. **B. Gueridi:** Validation.

Declaration of Competing Interest

All authors must disclose any actual or potential conflict of interest including any financial, personal or other relationships with other people or organizations within that could inappropriately influence (bias) their work. Examples of potential conflicts of interest which should be disclosed include employment, consultancies, stock ownership, honoraria, paid expert testimony, patent applications/registrations and grants and any other funding. Potential conflicts of interest should be disclosed when the article is submitted for consideration. The journal reserves the right to not publish an article on the basis of the declared conflict.

Data availability

No data was used for the research described in the article.

Acknowledgments

We would like to thank Taif University Research Supporting Project No. (TURSP-2020/66), Taif University, Taif, Saudi Arabia.

References

[1] N.A. Hill, K.M. Rabe, First-principles investigation of ferromagnetism and ferroelectricity in bismuth manganite, Phys. Rev. B 59 (1999) 8759–8769.
[2] R. Seshadri, N.A. Hill, Visualizing the Role of Bi 6s Lone Pairs in the Off-Center Distortion in Ferromagnetic $BiMnO_3$, Chem. Mater. 13 (2001) 2892–2899.
[3] F. Akram, R.A. Malik, S.A. Khan, A. Hussain, S. Lee, M.H. Lee, C.H. In, T.K. Song, W.J. Kim, Y.S. Sung, M.H. Kim, Electromechanical properties of ternary $BiFeO_3$−0.35$BaTiO_3$–$BiGaO_3$ piezoelectric ceramics, J. Electroceram. 41 (2018) 93–98.
[4] L. Krache, M.A. Ghebouli, B. Ghebouli, S. Alomairy, M. Reffas, M. Fatmi, T. Chihi, Phase stability, Electronic and Optical Properties in Pcca, R3c and Pm-3m phases of $BiGaO_3$ Perovskite, Phys. Status Solidi B (2022) 1–8.2200042.
[5] J.Z. Zhang, H.C. Ding, J.J. Zhu, Y.W. Li, Z.G. Hu, C.G. Duan, X.J. Meng, J.H. Chu, Electronic structure and optical responses of nanocrystalline $BiGaO_3$ films: A combination study of experiment and theory, J. Appl. Phys. 115 (2014), 083110.
[6] M. Guennou, P. Bouvier, GS. Chen, B. Dkhil, R. Haumont, G. Garbarino, J. Kreisel, Multiple high-pressure phase transitions in $BiFeO_3$, Phys. Rev. B. 84 (2011), 174107.
[7] S.A. Dar, M.A. Ali, V. Srivastava, Investigation on bismuth-based oxide perovskites MBiO3 (M= Rb, Cs, Tl) for structural, electronic, mechanical and thermal properties, Eur. Phys. J. B 93 (2020) 1–11.
[8] A.A. Bellik, T. Wuemischa, K. Mori, M. Maic, T. Nagai, Y. Matsui, E. Takayama-Muromachi, High-Pressure Synthesis, Crystal Structures, and Properties of Perovskite-like $BiAlO_3$ and Pyroxene-like $BiGaO_3$, Chem. Mater. 18 (2006) 133–139.
[9] J. Kaczkowski, Electronic structure, ferroelectric properties, and phase stability of $BiGaO_3$ under high pressure from first principles, J. Mater. Sci. 51 (2016) 9761–9770.
[10] J. Deb, D. Paul, U. Sarkar, Pentagraphyne: a new carbon allotrope with superior electronic and optical property, J. Mater. Chem. C 8 (2020) 16143–16150.
[11] J. Deb, U. Sarkar, Boron-nitride and boron-phosphide doped twin-graphene: Applications in electronics and optoelectronics, Appl. Surf. Sci. 541 (2021), 148657.
[12] P. Kumari, V. Srivastava, R. Khenata, S.A. Dar, S. Naqib, A first-principles prediction of thermophysical and thermoelectric performances of $SrCeO_3$ perovskite, Int. J. Energy Res. 46 (3) (2022) 2934–2946.
[13] K. Schwarz, P. Blaha, G.K.H. Madsen, Electronic structure calculations of solids using the WIEN2k package for material sciences, Comp. Phys. Commun. 147 (2002) 71–76.
[14] G.H.K. Madsen, D.J. Singh, A code for calculating band-structure dependent quantities, Comput. Phys. Commun. 175 (2006) 67–71.
[15] J.P. Perdew, K. Burke, M. Ernzerhof, Generalized gradient approximation made simple, Phys. Rev. Lett. 77 (1996) 3865–3868.
[16] JP. Perdew, A. Zunger, Self-interaction correction to density-functional approximations for many-electron systems, Phys Rev B 23 (1981) 5048–5079.
[17] P. Verma, D.G. Truhlar, HLE16: A local Kohn–Sham gradient approximation with good performance for semiconductor band gaps and molecular excitation energies, J. Phys. Chem. Lett. 8 (2017) 380–387.
[18] J. Heyd, G.E. Scuseria, M. Ernzerhof, Hybrid functionals based on a screened coulomb potential, J. Chem. Phys. 118 (2003) 8207–8215.
[19] F. Tran, P. Blaha, Accurate band gaps of semiconductors and insulators with a semilocal exchange-correlation potential, Phys. Rev. Lett. 102 (2009), 226401.
[20] A.D. Becke, E.R. Johnson, A Simple Effective Potential for Exchange 124, American Institute of Physics, 2006, 221101.
[21] V.I. Anisimov, O. Gunnarsson, Density-functional calculation of effective Coulomb interactions in metals, Phys. Rev. B 43 (1991) 7570–7574.
[22] S.B. Patel, A. Srivastava, R. Sharma, J.A. Abraham, V. Srivastava, Prediction of structural, electronic, mechanical, thermal, and thermoelectric properties in $PbMO_3$ (M= Sb, Bi) perovskite compounds: a DFT study, Eur. Phys. J. Plus 137 (2022) 380.
[23] M.A. Ghebouli, B. Ghebouli, L. Krache, S. Alomairy, M. Fatmi, T. Chihi, M. Reffas, Prediction study of the structural, elastic, electronic, dynamic, optical and thermodynamic properties of cubic perovskite $BiGaO_3$, Bull. Mater. Sci. 45 (2022) 1–11.
[24] B. Bhattacharya, J. Deb, U. Sarkar, Boron-phosphorous doped graphyne: a near-infrared light absorber, AIP Adv. 9 (2019), 095031.
[25] J. Deb, D. Paul, U. Sarkar, Density functional theory investigation of nonlinear optical properties of T-graphene quantum dots, J. Phys. Chem. A 124 (7) (2020) 1312–1320.